Optical Engineering

OpticalEngineering.SPIEDigitalLibrary.org

Design of stray light suppressed digital micromirror device-based spectrometer with compound parabolic concentrator

Xiangqian Quan
Hua Liu
Zhenwu Lu
Yongqian Quan
Xiaoduo Wang
Xinrong Hu
Hetuo Chen
Xiangquan Tan
Heyang Bu

SPIE.

Design of stray light suppressed digital micromirror device-based spectrometer with compound parabolic concentrator

Xiangqian Quan,[a,b] Hua Liu,[a,*] Zhenwu Lu,[a] Yongqian Quan,[c] Xiaoduo Wang,[a,b] Xinrong Hu,[a,b] Hetuo Chen,[d] Xiangquan Tan,[a] and Heyang Bu[b]
[a]Chinese Academy of Sciences, Changchun Institute of Optics, Fine Mechanics and Physics, Changchun 130033, China
[b]University of Chinese Academy of Sciences, Changchun Institute of Optics, Fine Mechanics and Physics, Beijing 100049, China
[c]CRRC Corporation Limited, Zhuzhou Times Material Technology, Co. Ltd., Zhuzhou 412007, China
[d]University of Electronic Science and Technology of China, School of Microelectronics and Solid-state Electronics, Chengdu 610054, China

Abstract. To suppress the stray light caused by the diffraction and scattered light of a digital micromirror device (DMD) in a DMD-based spectrometer, a new concentrator system with a compound parabolic concentrator (CPC) is presented, which has the advantage that all stray light beyond the acceptance angle can be rejected with the most compact device available. The diffraction of DMD is explored to determine the acceptance angle, and the parameters of the concentrator system are analyzed to determine the geometric concentration ratio. The simulation results show that the spectrum concentration efficiency of the CPC is 98.7%, that the stray light concentration efficiency from the DMD is 36.3%, and that the stray light concentration efficiency beyond the acceptance angle is 0.00%. Finally, according to the discussion about tolerance on the CPC, a conclusion can be drawn that the new DMD-based spectrometer with CPC is feasible and significant in suppressing the stray light. [DOI: 10.1117/1.OE.54.11.115101]

Keywords: diffraction theory; spectrometers; concentrators; digital micromirror device; stray light.

Paper 150843 received Jun. 21, 2015; accepted for publication Sep. 14, 2015; published online Nov. 2, 2015.

1 Introduction

In recent years, as its several potential advantages over a common spectrometer, such as lower cost, higher resolution and light capture efficiency, and wider spectral range, have been demonstrated by Kearney and Ninkov,[1,2] the spectrometer based on a digital micromirror device (DMD) has been widely investigated.[3,4] An affordable spectrometer based on a DMD in the near-infrared region from 1.35 to 2.450 μm was developed at Texas Instruments.[5] Sun et al.[6,7] developed an engineering prototype of Hadamard transform spectral imager based on DMD. But along with the advantages of the DMD, disadvantages including diffraction and scattered light caused by the microstructure of the DMD also introduced stray light at the same time.[8–10]

In our research team, Wang et al.[11] designed a DMD-based spectrometer in the near-infrared band, where the concentrator system was designed with a conventional converging lens. Because of the stray light of the DMD, the precision of the measurement was reduced accordingly. Kenneth et al. have carried out a series of measurements of the stray light of a DMD to determine the optical design parameters.[12–14] Rose et al. introduced a light-absorbing dump to reduce the diffraction light of "off" state light.[15,16] But the diffraction light beyond the dump and scattered light still existed and caused great anomalies in the spectral response.

In this paper, the experimental apparatus of a DMD-based spectrometer is established to test the stray light. Then a new concentrator system with a compound parabolic concentrator (CPC) is presented according to the design principle of nonimaging optics. By exploring the diffraction of the DMD, the acceptance angle of the CPC is determined. By analyzing the concentrator system, the geometric concentration ratio is determined. Eventually, a DMD-based spectrometer with a CPC in the spectrum region from 1.1 to 1.7 μm is designed. According to the simulation results, the stray light concentration is less than the spectrum concentration efficiency. Finally, based on a Monte Carlo method, three types of tolerances on the CPC are discussed, including material tolerance, machining tolerance, and alignment tolerance. A conclusion can be drawn that the concentrator system with the CPC is significant and feasible in suppressing the stray light.

2 Theory and Method

The configuration of the DMD-based spectrometer is shown in Fig. 1. Polychromatic light from fiber is collimated by the collimating lens. The collimated light is split by the grating and focused onto the DMD by the imaging lens. After encoding by the DMD according to the modulated pattern, the different spectrum components are concentrated onto the single detector by the converging lens. Eventually, the spectra are decoded and displayed by the computer. The concentrator system is designed with a lens, and the diffraction and scattering of the DMD introduce the stray light.[11]

An experimental apparatus of stray light measurement is shown as Fig. 2. Passing through the sample pool, the light source illuminates the slit. By passing the near-infrared bandpass filter, only the light component in the near-infrared

*Address all correspondence to: Hua Liu, E-mail: liuhua_rain@aliyun.com

0091-3286/2015/$25.00 © 2015 SPIE

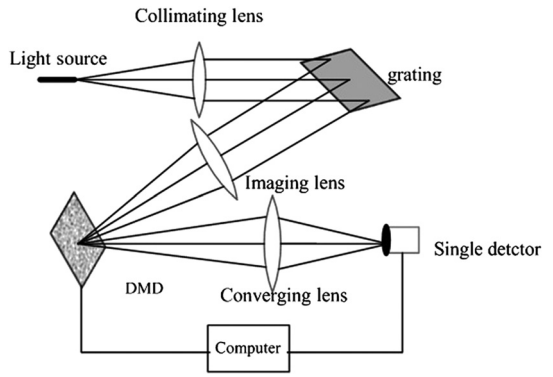

Fig. 1 Schematic diagram of a digital micromirror device (DMD)–based spectrometer.

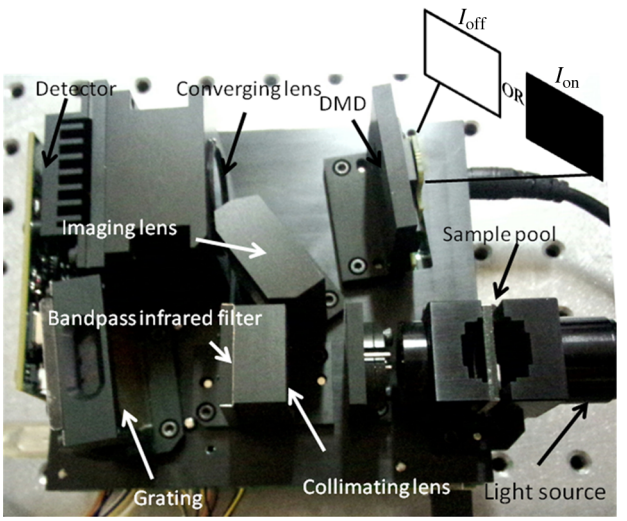

Fig. 2 Experimental apparatus for measurement of stray light.

region remains. After being collimated by the collimating lens, the light is split by the grating and focused onto the DMD by the imaging lens. Finally, encoded by the DMD according to the modulated pattern, the different spectrum components are concentrated onto the single detector by the converging lens. The single grating has a groove density of 300 lines/mm. The spectrum range covers from 1.35 to 2.45 μm. When all mirrors are in the "on" state, the relative intensity I_{on} (which has not been calibrated) is detected. When all mirrors are in the "off" state, the relative intensity I_{off} (which has not been calibrated) is detected.

The contrast value C (the ratio of I_{off} to I_{on}) is shown as Table 1.

The diffraction of the DMD can be described as in Fig. 3. The monochromatic light strikes on the DMD with a wavelength of 632.8 nm and incident angle of 24 deg. In the DMD-based spectrometer, the diffraction orders within the

Table 1 Contrast of stray light to spectrum.

I_{off}	I_{on}	C
2689162	1627352484	0.17%

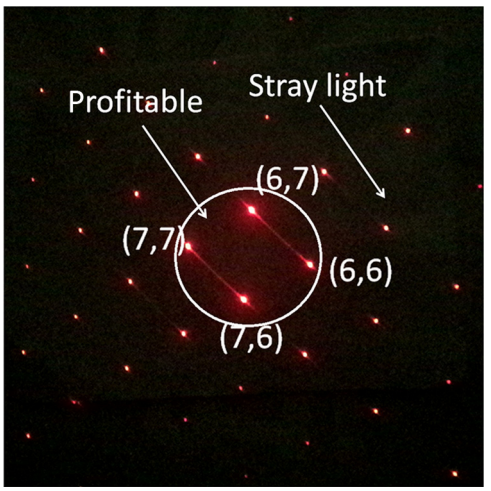

Fig. 3 Diffraction of the DMD at a wavelength of 632.8 nm.

(0,0) order diffraction of a single micromirror are (6,6), (6,7), (7,6), and (7,7), which are profitable for spectrum detection. And the stray light consists of diffraction of the "on" state or "off" state, the scattered light of the DMD, and background light.

To design a concentrator system to suppress stray light, a nonimaging optical design that has fewer design freedom is adopted. One of the nonimaging concentrating devices is the CPC, which is based on the edge optical principle, in which the light within the acceptance angle arrives at the detector surface through multireflection and the stray light beyond the acceptance angle is rejected with the most compact structure.[17–22] The concentration phenomena of the CPC are shown in Fig. 4. The beams within θ are concentrated by the CPC, and the beams beyond θ are rejected.

Besides the acceptance angle, another factor that should be considered in the design of the CPC is the geometric concentrating ratio C. The relationship between the acceptance angle and concentration ratio can be described as in Eq. (1):

$$C < 1/\sin^2(\theta), \tag{1}$$

where C is the geometric concentrating ratio and θ is the acceptance angle. The relationships of the design parameters of the CPC are described in Eq. (2):[23]

$$\left.\begin{aligned} f &= R(1+\sin\theta) \\ L &= f\cos\theta/\sin^2\theta \end{aligned}\right\}, \tag{2}$$

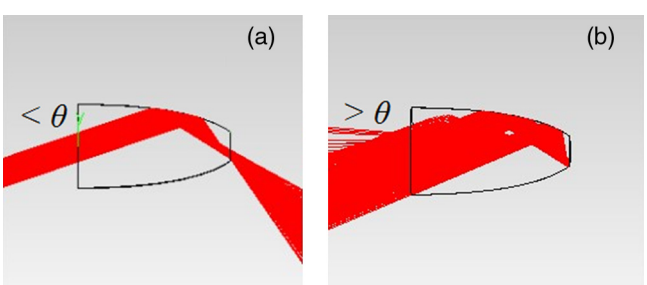

Fig. 4 Concentration phenomenon of CPC: (a) the beams within the acceptance angle θ are concentrated by the CPC. (b) The beams beyond the acceptance angle θ are rejected.

where f is the focal length, R is the lateral focal (half of the exit aperture diameter of CPC), and L is the front length.

3 Specific Parameters

3.1 *Determine the Acceptance Angle of Compound Parabolic Concentrator*

The single micromirror diffraction I' is described by Eq. (3):[24,25]

$$\begin{cases} I' = I_0 \operatorname{sinc}^2 u' \operatorname{sinc}^2 u'' \\ u' = \frac{\pi a}{\lambda}\left[(\sin\alpha\cos\beta - \sin\alpha_0\cos\beta_0) + \frac{\tan\varphi}{\sqrt{2}}(\cos\alpha - \cos\alpha_0)\right], \\ u'' = \frac{\pi a}{\lambda}\left[(\sin\alpha\sin\beta - \sin\alpha_0\sin\beta_0) + \frac{\tan\varphi}{\sqrt{2}}(\cos\alpha - \cos\alpha_0)\right] \end{cases} \tag{3}$$

where u' and u'' determine the diffraction angle of a single micromirror from two directions, λ is the wavelength, α is the angle of diffracted light, α_0 is the angle of incident light with one side of the DMD, β is the angle of diffracted light and β_0 the angle of incident light with the normal of the DMD, φ is the rotating angle of the micromirror along its diagonal, and a is the side length of the micromirror.

The multiple micromirror interference I'' is described by Eq. (4):

$$\begin{cases} I'' = \frac{\sin^2[(2M)\nu']\sin^2[(2N)\nu'']}{\sin^2\nu'\sin^2\nu''} \\ \nu' = \frac{\pi a}{\lambda}(\sin\alpha\cos\beta - \sin\alpha_0\cos\beta_0), \\ \nu'' = \frac{\pi a}{\lambda}(\sin\alpha\sin\beta - \sin\alpha_0\sin\beta_0) \end{cases} \tag{4}$$

where M and N are the number of interference micromirrors in two directions. Then the corresponding energy distribution of DMD diffraction is shown by Eq. (5),

$$I = I'I''. \tag{5}$$

The DMD consists of 1024×768 micromirrors, which are 13.68 μm $\times$ 13.68 μm square mounted on a 14.68 μm pitch. The micromirrors can rotate either +12 deg or −12 deg along the diagonal direction. The diffractions of the DMD at wavelengths of 1.1 μm, 1.4 μm, and 1.7 μm can be derived as Figs. 5(a)–5(c). The horizontal axis represents the diffraction angle along the diagonal direction, and the longitudinal axis represents diffraction efficiency. Curve a presents the diffraction of a single micromirror. Curve b presents the interference of multiple micromirrors. Curve c presents the diffraction of the whole DMD by modulating curve b by curve a. The (0,0) order interference position of multiple micromirrors is 24 deg, and the (0,0) order diffraction position of single micromirror is 0 deg. The single micromirror diffraction angle increases along with the wavelength, which reaches approximately 9 deg at 1.7 μm.

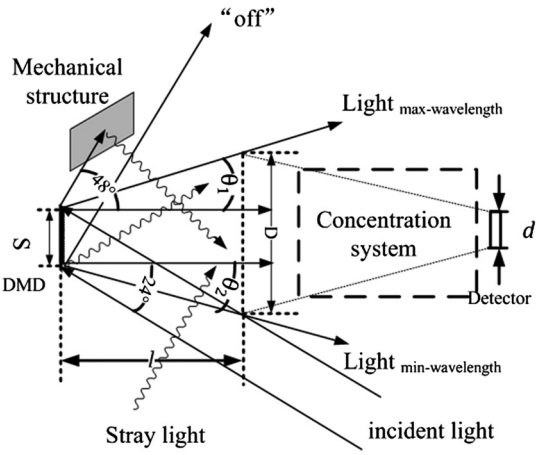

Fig. 6 Design schematic of the concentrator system.

3.2 *Determine the Geometric Concentrating Ratio of Compound Parabolic Concentrator*

To determine the geometric concentrating ratio of the CPC, the design parameters of the concentrator system are analyzed as in Fig. 6. The incident spectra are focused on the DMD at 24 deg. The (0,0) order diffraction of the "on" state is centered at 0 deg, and the (0,0) order diffraction of the "off" state is centered at 48 deg. The stray light includes the scattering light of the DMD, the reflected light of the mechanical structure, and background light. The diffraction of the DMD and the size of the detector determine the design parameters of the concentrator system.

The geometric concentrating ratio of the concentrator system is derived as in Eq. (6),

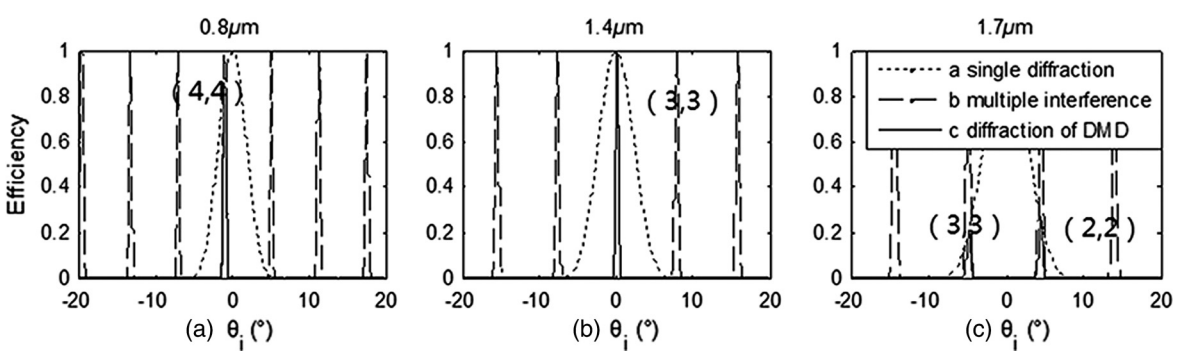

Fig. 5 Diffraction efficiency of the DMD: (a) When $\lambda = 1.1$ μm, the brightest interference order is (4,4) and the single-pixel diffraction angle is 6 deg. (b) When $\lambda = 1.4$ μm, the brightest interference order is (3,3) and the single-pixel diffraction angle is 7.5 deg. (c) When $\lambda = 1.7$ μm, the brightest interference order is (2,2) and the single-pixel diffraction angle is 9 deg.

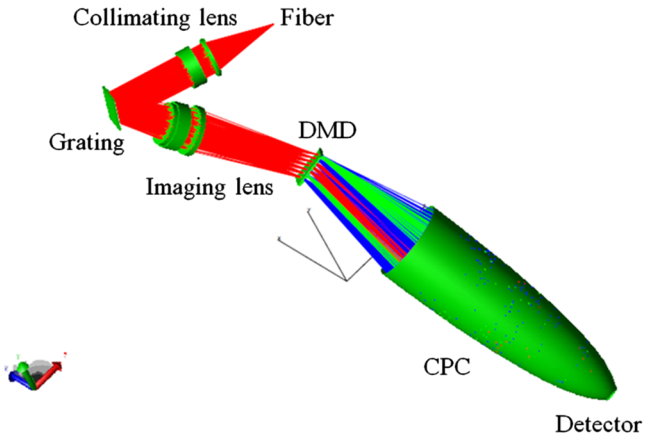

Fig. 7 Model of the DMD-based spectrometer in the TracePro program.

$$\left.\begin{aligned} C &= D/d \\ D &= S + l(\tan\theta_2 + \tan\theta_1) \\ l\ \tan 24\ \deg &= l\ \tan\theta_2 + S \end{aligned}\right\}, \tag{6}$$

where C is the geometric concentrating ratio, D is the entrance aperture diameter of the concentrator system, d is the diameter of a single detector, S is the diagonal length of the DMD, l is the distance between the DMD and concentrator system, and θ_1 and θ_2 are the angle ranges of the (0,0) order of single micromirror diffraction at the maximum and minimum wavelengths, respectively.

3.3 *Design a Digital Micromirror Device-Based Spectrometer with Compound Parabolic Concentrator*

Figure 7 shows the model of a DMD-based spectrometer with CPC. Polychromatic light from the fiber is collimated by the collimating lens. The collimated light is split by a grating with incident angle of 12.6 deg and focused onto the DMD by an imaging lens with incident angle of 24 deg. Two orthogonal transmission gratings are adopted to achieve the same diffraction as the DMD. The spectrum range is from 1.1 μm to 1.7 μm. The numerical aperture (NA) of the fiber is 0.22, and the diameter of the fiber is 100 μm. A 0.7 × GA DMD chip with 13.68 μm × 13.68 μm micromirrors and ± 12 deg tilt angle is adopted. The dimension of the grating is 12.8 mm × 12.8 mm with a groove density of 300 lines/mm and blazing wavelength of 1.3 μm. The spectrum resolution on the DMD is superior to 5.5 nm. According to the analysis of the diffraction angle of a single micromirror at 1.7 μm, the acceptance angle should be 9 deg. On the basis of Eq. (6), the entrance aperture diameter of the CPC should be 31.1 mm. Since the radius of a single detector is 3 mm, the concentrating ratio should be greater than 5.2. On the basis of Eq. (1), the concentrating ratio of 6.4 and axis tilt of 9 deg are adopted. The back length is set to be 0 mm for compactness and stray light suppression. The CPC is designed with a hollow reflective form. According to Eq. (2), the focal length should be 3.47 mm, the front length should be 140 mm, and the lateral focal length is 2.99 mm. The spectroscopic image of the slit is focused onto the DMD with light incident at 24 deg. The radius of a single point detector is 3 mm.

4 Results and Discussion

4.1 *Spectral Energy Efficiency in Digital Micromirror Device-Based Spectrometer with Compound Parabolic Concentrator*

Figure 8 shows the irradiance maps for the DMD and detector in the DMD-based spectrometer with CPC. Each spot represents the spectrum irradiance at wavelengths of 1.1 μm to 1.7 μm with an interval of 0.1 μm. Figure 8(a)

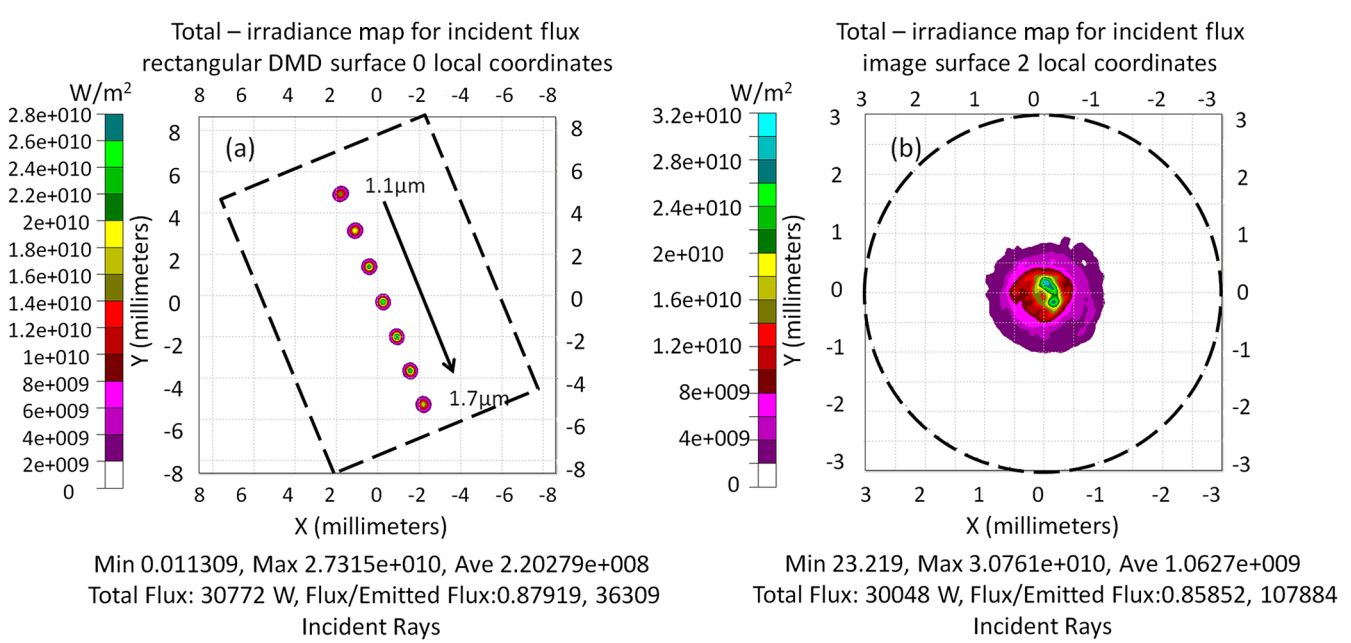

Fig. 8 Irradiance maps in the DMD-based spectrometer with CPC: (a) irradiance map on the DMD; (b) irradiance map on the detector.

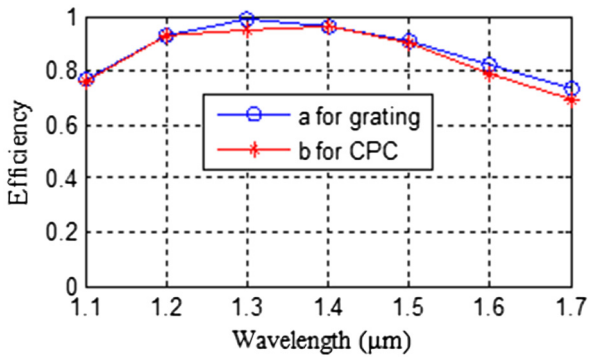

Fig. 9 Spectral energy efficiencies in the spectrometer. The horizontal axis represents the wavelength in millimeters, and the longitudinal axis represents spectral energy efficiency. Curve a represents the diffraction efficiency of grating. Curve b represents the spectral response of spectrometer with CPC.

shows that the ratio of the flux on the DMD to the emitted flux of the source is 0.8719, and Fig. 8(b) shows that the ratio of the flux on the detector to the emitted flux of the source is 0.85852.

The spectral energy efficiency on the target surface is calculated by[22]

$$E = P_{\text{detected}}/P_{\text{incident}}, \tag{7}$$

where E is the spectral energy efficiency on the target surface, P_{detected} is the detected flux on the target surface, and P_{incident} is the incident flux of the system. In the circumstance of discussing the spectral energy efficiency of the spectrometer, P_{detected} is the flux on the surface of the detector and P_{incident} is the emitted flux of the source.

As shown in Fig. 9, curve *a* indicates the diffraction efficiency of the grating, which reaches the maximum at 1.3 μm and determines the max spectral energy efficiency of spectrometer. Curve *b* indicates the spectral energy efficiency on the detector in the spectrometer with CPC. It is shown that the spectral energy efficiency with CPC is close to the diffraction efficiency of the grating in the entire spectrum region.

As shown in Fig. 10, (a) is the irradiance map on the entrance surface of the CPC, which indicates that the spectral energy efficiency is 87.0%. (b) is the irradiance map on the surface of the detector, which indicates that the spectral energy efficiency is 85.9%.

The concentrating efficiency of the concentrator system with CPC can be derived by[22]

$$\eta = E_{\text{detector}}/E_{\text{CPC}}, \tag{8}$$

where η is the concentration efficiency of the concentrator system, E_{detector} is the spectral energy efficiency on the surface of the detector, and E_{CPC} is the spectral energy efficiency on the entrance surface of the CPC. The concentration efficiency of spectrum η_{spectrum} {the ratio of E_{detector} [shown as Fig. 10(a)] to E_{CPC} [shown as Fig. 10(b)]} is derived. It is shown that the spectral concentration efficiency of the CPC is 98.7% and closes to the perfect energy transmission efficiency. In addition, the energy distribution is concentrated within a small region.

4.2 *Concentration Efficiency of Stray Light*

When the stray light from the DMD is simulated in accordance with the Lambertian, the spectral irradiance maps on the entrance of the CPC and detector are as shown in Fig. 11. (a) indicates that the spectral energy on the entrance of the CPC is 9.93%; (b) indicates that the spectral energy on the detector is 3.60%. According to Eq. (8), the concentration efficiency of stray light [the ratio of the energy efficiency of Fig. 11(b) to the energy efficiency of Fig. 11(a)] from the DMD is 36.3%.

Since the stray light of the background or refraction is too complex to be simulated, we only discuss the beam with an

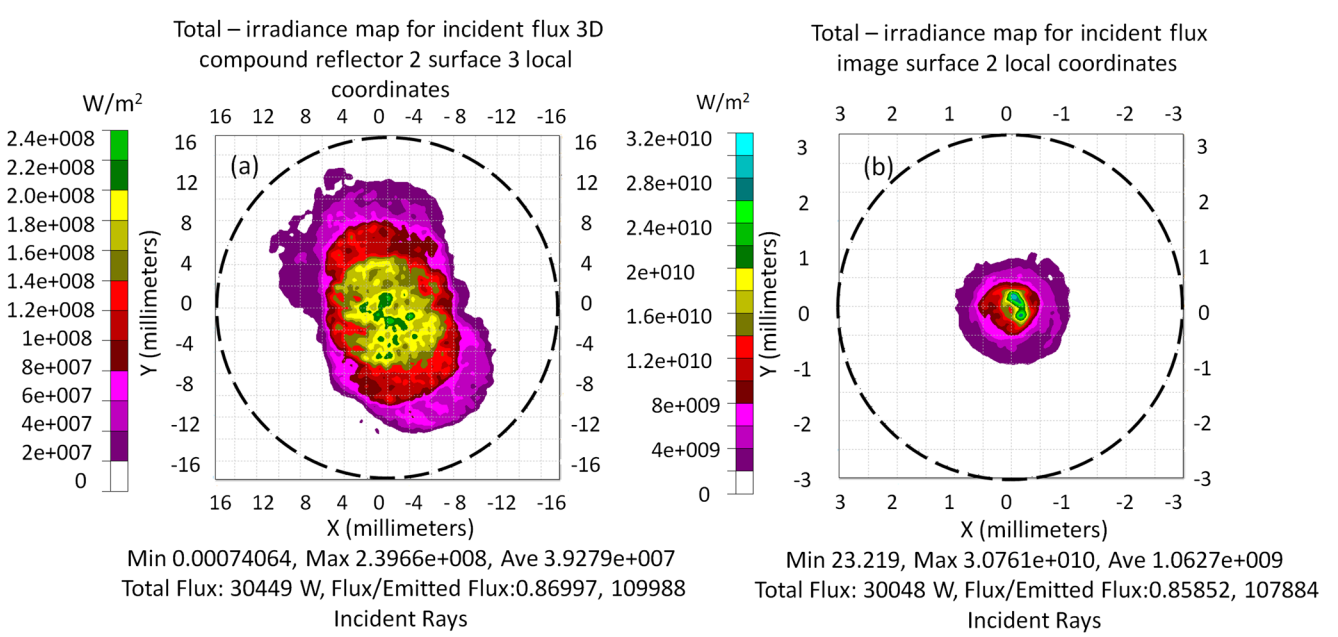

Fig. 10 Spectrum concentration efficiency of the CPC: (a) spectrum irradiance map on the entrance of the CPC and (b) spectrum irradiance map on the detector.

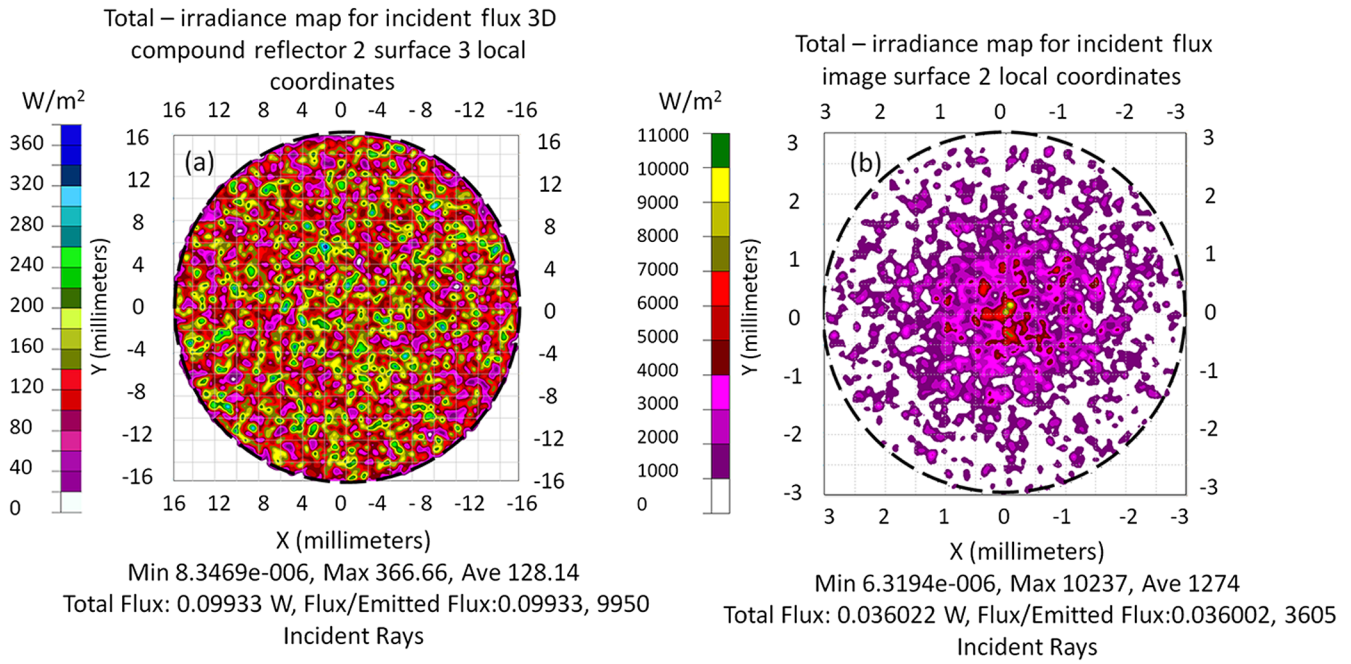

Fig. 11 Concentration efficiency of stray light from the DMD: (a) the irradiance map of stray light from the DMD on the entrance of the CPC and (b) irradiance map of stray light from the DMD = on the detector.

incident angle of 10 deg, which is beyond the acceptance angle of 9 deg. Figure 12(a) shows the irradiance map on the entrance of the CPC with a spectral energy of 100%. (b) shows the irradiance map on the surface of the detector with a spectral energy of 0.00% of the total energy. According to Eq. 8, the stray light concentration efficiency with an incident angle of 10 deg [the ratio of the energy efficiency of Fig. 12(b) to the energy efficiency of Fig. 12(a)] is 0.00%.

Eventually, the comparison of the concentration efficiencies of spectrum and stray light is as shown in Table 2. The concentration efficiencies of the two types of stray light are less than that of the spectrum. A conclusion can be drawn that the concentrator system of the CPC is feasible and significant in suppressing the stray light.

4.3 *Discussion of Tolerance on the Compound Parabolic Concentrator*

Three types of variable tolerances are discussed, including machining tolerance, material tolerance, and alignment tolerance.[26] Three tolerance design functions are analyzed

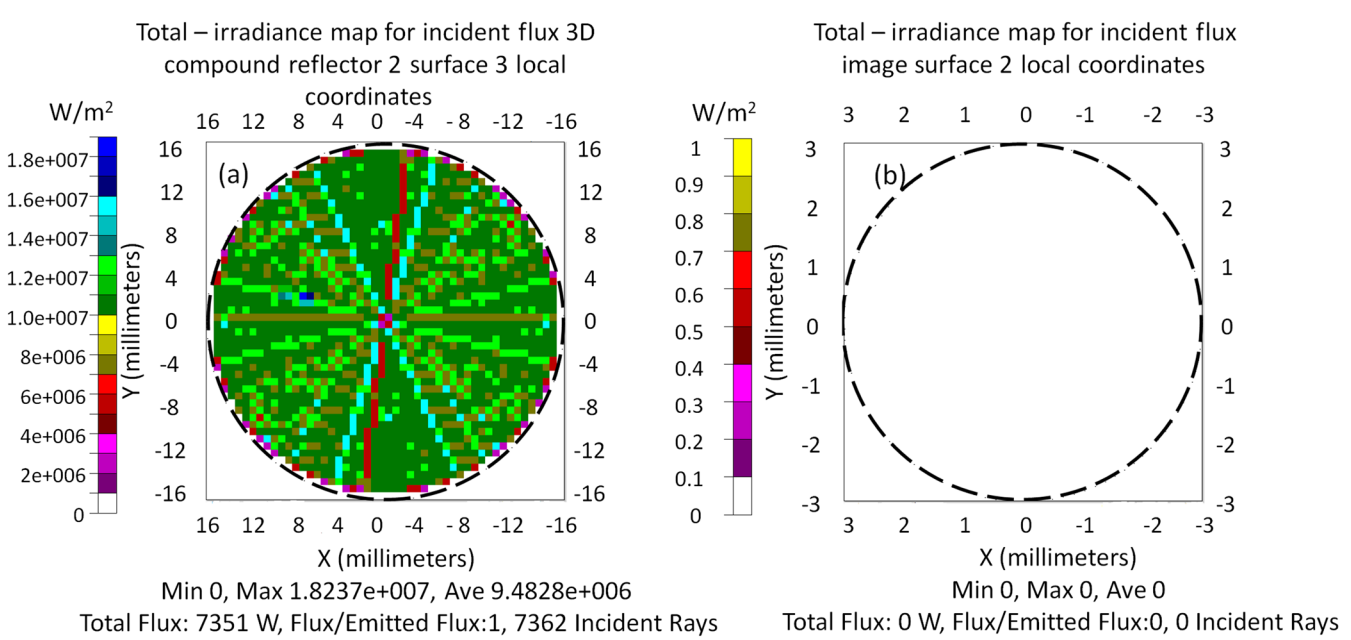

Fig. 12 Concentration efficiency of stray light beyond the acceptance angle: (a) irradiance map of stray light with the incident angle of 10 deg on the entrance of the CPC and (b) the irradiance map of stray light with an incident angle of 10 deg on the detector.

Table 2 Comparison of the concentration efficiency of spectrum and stray light.

	Efficiency on the entrance of CPC	Efficiency on the detector	The concentration efficiency (%)
η_{spectrum}	87.0	85.9	98.7
$\eta_{\text{straylight\_DMD}}$	9.93	3.60	36.3
$\eta_{\text{straylight\_}\theta i=10\ \text{deg}}$	100	0.00	0.00

including the stray light concentration efficiency of the DMD, $\eta_{\text{straylight\_DMD}}$; the stray light concentration efficiency with $\theta_i = 10$ deg, $\eta_{\text{straylight\_}\theta i=10\ \text{deg}}$; and spectrum concentration efficiency η_{spectrum}. For the machining tolerance of the CPC, the acceptance angle θ and lateral focal length R are the main variable tolerances. For the material tolerance of the CPC, the reflective efficiency of the material r_1 is the main variable tolerance. The alignment tolerance has two parts including the alignment tolerance of the CPC and the alignment tolerance of the detector. The model of thealignment tolerance discussion is shown in Fig. 13. A Cartesian coordinate system is established in which the center of the DMD is set as the origin. Due to the symmetry of the optical system, the alignment tolerances of the CPC and detector have three variables. The eccentric errors of the CPC and detector in the X direction are defined as e_1 and e_2, respectively; the location errors of the CPC and detector in the Z direction are defined as L_1 and L_2, respectively; and the axis tilt errors of the CPC and detector with the Z axis are defined as t_1 and t_2, respectively.

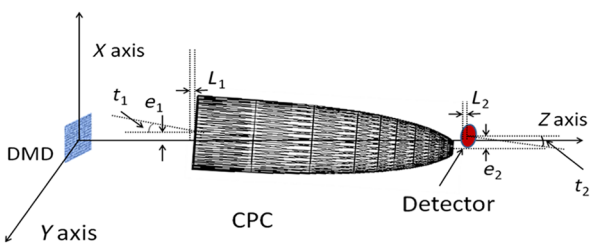

Fig. 13 Model of tolerance analysis of the CPC.

Table 4 Distribution of variable tolerances.

Variable tolerances	Expectation	Standard deviation
θ	9	0.2
R	3	0.2
r_1	0.975	0.1
e_1	0	2
L_1	0	5
t_1	0	0.2
e_2	0	0.2
L_2	0	0.2
t_2	0	2

When the variables change, the spectrum concentration efficiency, η_{spectrum}, the stray light concentration efficiency of the DMD, $\eta_{\text{straylight\_DMD}}$, and the stray light concentration efficiency with $\theta_i = 10$ deg can be derived. According to the process level and restriction of $\eta_{\text{spectrum}} > 0.95$, $\eta_{\text{straylight\_DMD}} < 0.4$, and $\eta_{\text{straylight\_}\theta_i=10^\circ} = 0$, the preset variable tolerances and the corresponding variation ranges of η_{spectrum}, $\eta_{\text{straylight\_DMD}}$, and $\eta_{\text{straylight\_}\theta i=10\ \text{deg}}$ are shown as Table 3.

Since the uncertainty of the process and the alignment is related to process capability, assembly environment, or other conditions, we consider the variation ranges of each variable tolerance as being accordance with the Gaussian distribution. The expectations and standard deviations are preset as in Table 4.

Based on a Monte Carlo simulation method, the performance of the concentrator system with CPC in the DMD-based spectrometer is analyzed. When 100 samples are simulated in the TracePro program, the statistical results of samples are as shown in Table 5.

Table 3 Preset variable tolerances and the corresponding variation ranges of tolerance design functions.

Category	Variable tolerances	Preset value	η_{spectrum}	$\eta_{\text{straylight\_DMD}}$	$\eta_{\text{straylight\_}\theta i=10\ \text{deg}}$
Machining tolerance	θ	9 ± 0.5 deg	[0.966,0.987]	[0.304,0.404]	[0,0]
	R	3 ± 0.5 mm	[0.959,0.987]	[0.297,0.363]	[0,0]
Material tolerance	r_1	$1 + 0/-0.5$	[0.938,0.987]	[0.341,0.363]	[0,0]
Alignment tolerance	e_1	0 ± 5 mm	[0.951,0.987]	[0.329,0.363]	[0,0]
	L_1	0 ± 10 mm	[0.978,0.987]	[0.348,0.370]	[0,0]
	t_1	0 ± 0.5 deg	[0.977,0.987]	[0.355,0.363]	[0,0]
	e_2	0 ± 0.5 mm	[0.963,0.987]	[0.342,0.363]	[0,0]
	L_2	0 ± 0.5 mm	[0.964,0.987]	[0.321,0.403]	[0,0]
	t_2	0 ± 2 deg	[0.986.0.987]	[0.361,0.363]	[0,0]

Table 5 Statistical results of simulations.

	Notional value	Optimal values	Worst value	Average value	Standard deviation
η_{spectrum}	0.9868	0.9844	0.8928	0.9483	0.0167
$\eta_{\text{straylight\_DMD}}$	0.3635	0.2407	0.4149	0.3394	0.0289
$\eta_{\text{straylight\_}\theta i=10\ \text{deg}}$	0	0	0	0	0

Table 6 Distribution of η_{spectrum} and $\eta_{\text{straylight}}$.

Sample proportion	90%	80%	50%	20%	10%
η_{spectrum}	>0.9279	>0.9377	>0.9486	>0.9639	>0.9672
$\eta_{\text{straylight\_DMD}}$	<0.3772	<0.3661	<0.3388	<0.3194	<0.3062
$\eta_{\text{straylight\_}\theta i=10\ \text{deg}}$	0	0	0	0	0

The distributions of η_{spectrum}, $\eta_{\text{straylight\_DMD}}$, and $\eta_{\text{straylight\_}\theta i=10\ \text{deg}}$ are shown in Table 6.

5 Conclusion

To eliminate the stray light caused by the diffraction and scattering of the DMD, a new concentrator system with a CPC is presented to replace the conventional lens. By analyzing the diffraction of the DMD, the acceptance angle of the CPC is derived. By analyzing the entrance aperture sizes of the CPC and detector, the geometric concentrating ratio is derived. Then, a DMD-based spectrometer with CPC is designed. The simulation results show that the spectral energy efficiency of the detector is close to the diffraction efficiency of the grating at different wavelengths. And the simulation results also show that the spectrum concentration efficiency of theCPC is 98.7%, that the stray light concentration efficiency of the DMD is 36.3%, and that the concentration efficiency of stray light beyond the acceptance angle is 0.00%. According to the simulation results based on the Monte Carlo method, 90% of the simulation optical systems show that the spectrum concentration efficiency is superior to 93.79%, that the stray light concentration efficiency of the DMD is less than 37.72%, and that the stray light concentration efficiency with $\theta_i = 10$ deg is 0.00%. Then, a conclusion can be drawn that the new concentrator system with CPC is feasible and significant in concentrating the spectrum and suppressing the stray light. In addition, the spectral energy distribution is concentrated in a smaller region, and the optical structure is compact.

Acknowledgments

This work was supported by the National Natural Science Foundation of China under Grant No. 61137001 and the Projects of Science and Technology Development Plan of Jilin Province under Grant No. 20130206018GX.

References

1. T. Hirschfeld and G. Wyntjes, "Fourier transform vs Hadamard transform spectroscopy," *Appl. Opt.* **12**(12), 2876–2880 (1973).
2. K. J. Kearney and Z. Ninkov, "Characterization of a digital micro mirror device for use as an optical mask in imaging and spectroscopy," *Proc. SPIE* **3292**, 81–92 (1998).
3. N. Goldstein et al., "DMD-based adaptive spectral imagers for hyperspectral imagery and direct detection of spectral signatures," *Proc. SPIE* **7210**, 721008 (2009).
4. T. Hirschfeld and G. Wyntjes, "Fourier transform vs Hadamard transform spectroscopy," *Appl. Opt.* **12**(12), 2876–2880 (1973).
5. Texas Instruments, "DLP® NIRscan™ Evaluation Module (EVM) User's Guide," (2014), http://www.ti.com/lit/ug/dlpu016b/dlpu016b.pdf.
6. X. Sun et al., "An engineering prototype of Hadamard transform spectral imager based on Digital Micro-mirror Device," *Opt. Laser Technol.* **44**, 210–217 (2012).
7. D. Shrekenhamer, C. Watts, and W. Padilla, "Terahertz single pixel imaging with an optically controlled dynamic spatial light modulator," *Opt. Express* **21**(10), 12507–12518 (2013).
8. X. Ding et al., "Microscopic lithography with pixelate diffraction of a digital micro-mirror device for micro-lens fabrication," *Appl. Opt.* **53**(24), 5307–5311 (2014).
9. Z. Xiong et al., "Diffraction analysis of digital micromirror device in maskless photolithography system," *J. Micro/Nanolith. MEMS MOEMS.* **13**(4), 043016 (2014).
10. D. Xiang and M. A. Arnold, "Solid-state digital micro-mirror array spectrometer for hadamard transform measurements of glucose and lactate in aqueous solutions," *Appl. Spectrosc.* **65**(10), 1170–1180 (2011).
11. X. Duo Wang et al., "Design of a spectrum-folded Hadamard transform spectrometer in near-infrared band," *Opt. Commun.* **333**(15), 80–83 (2014).
12. K. D. Fourspring, Z. Ninkov, and J. P. Kerekes, "Scattered light in a DMD-based multi-object spectrometer," *Proc. SPIE* **7739**, 77393X (2010).
13. J. P. Rice et al., "DMD diffraction measurements to support design of projectors for test and evaluation of multispectral and hyper-spectral imaging sensors," *Proc. SPIE* **7210**, 72100D (2009).
14. B. Rose et al., "Programmable spectroscopy enabled by DLP," *Proc. SPIE* **9376**, 93760I (2015)
15. J. Xu, B. Hu, and D. Feng, "The correction of recovered spectral images in a Hadamard transform spectral imager based on a digital micro-mirror device" *Appl. Spectrosc.* **66**(9), 1044–1052 (2012).
16. J. P. Rice et al., "DMD diffraction measurements to support design of projectors for test and evaluation of multispectral and hyper-spectral imaging sensors," *Proc. SPIE* **7210**, 72100D (1998).
17. J. M. Gordon, "Complementary construction of ideal non-imaging concentrators and its applications," *Appl. Opt.* **35**(28), 5677–5682 (1996).
18. A. Suzuki and S. Kobayashi, "Absorber design for a compound parabolic concentrator collector without transmission loss," *Appl. Opt.* **33**(28), 6578–6581 (1994).
19. J. M. Gordon and A. Rabl, "A Non-imaging compound parabolic concentrator-type reflectors with variable extreme direction," *Appl. Opt.* **31**(34), 7332–7338 (1992).
20. J. Fang et al., "Compound parabolic concentrator applied as receiving antenna in scattering optical communication," *Chin. Opt. Lett.* **8**(5), 478–481 (2010).
21. E. D. Kosten et al., "Highly efficient GaAs solar cells by limiting light emission angle," *Light Sci. Appl.* **2**, e45 (2013).
22. D. Suresh, J. O'gallagher, and R. Winston, "Thermal and optical performance test results for compound parabolic concentrators (CPCs)," *Sol. Energy* **44**(5), 257–270 (1990).

23. W. T. Welford and R. Winston, *High Collection Non-imaging Optics*, Academic, New York (1989).
24. B. Lee, "DMD 101: Introduction to digital micromirror device (DMD) technology," (2013), http://www.ti.com/lit/an/dlpa008a/dlpa008a.pdf.
25. X. Chen et al., "Diffraction of digital micro-mirror device gratings and its effect on properties of tunable fiber lasers," *Appl. Opt.* **51**(30), 7214–7220 (2012).
26. N. Sellami, T. K. Mallick, and D. A. McNeil, "Optical characterisation of 3-D static solar concentrator," *Energy Conver. Manag.* **64**, 579–586 (2012).

Xiangqian Quan is a PhD student in the University of the Chinese Academy of Sciences. He received his BS degree in physics from the Northeast Forestry University in 2011. His current research interests include spectrometer design and image processing.

Hua Liu is a researcher at the Changchun Institute of Optics, Fine Mechanics and Physics, Chinese Academy of Sciences. He received his PhD from the University of the Chinese Academy of Sciences in 2006. His current research interests include nonimaging optical design and precision measurement.

Zhenwu Lu is a researcher at Changchun Institute of Optics, Fine Mechanics and Physics, Chinese Academy of Sciences. He received his master's degree from the University of the Chinese Academy of Sciences in 1985. His current research interests include binary optics, nonimaging optical design, and precision measurement.

Yongqian Quan is an engineer at Zhuzhou Times Material Technology, Co. Ltd. He received his bachelor's degree in traffic equipment and information engineering from the Central South University in 2007. His current research interests include precision measurement and imaging processing.

Xiaoduo Wang is a PhD student in the University of Chinese Academy of Sciences. She received her bachelor's degree in optical information science and technology from the Ocean University of China in 2011. Her current research interests include optical design and spectrometry.

Xinrong Hu completed his BS degree in optical information science and technology at Northwestern Polytechnical University in 2010 and his PhD at the University of the Chinese Academy of Sciences in 2015. Currently, he is a research assistant in the Space Photonics Information Technology Research Department at Xi'an Institute of Optics and Precision Mechanics, Chinese Academy of Sciences. His current research interests include optical system design and optical testing.

Hetuo Chen is a PhD student in the University of Electronic Science and Technology of China. He received his BS degree in physics from the Northeast Forestry University in 2011. His current research interests include electronic information processing.

Xiangquan Tan is an assistant researcher at the Optoelectronics Research Center of the Changchun Institute of Optics, Fine Mechanics and Physics, Chinese Academy of Sciences. He received his BS and MS degrees in mechanical engineering from Harbin Engineering University, China, in 2008 and 2011, respectively. His current research interests include optomechanical systems design and robotic system design.

Heyang Bu is a research trainee at Changchun Institute of Optics, Fine Mechanics and Physics, Chinese Academy of Sciences. He has been engaged in research of coronagraphy and optical design and has participated in many scientific research projects. His current research interests include ground-based coronagraphy and space coronagraphy.